SAND REPORT

SAND2002-8333
Unlimited Release
Printed August 2002

Pressure Waves Induced by Megasonic Agitation in a LIGA Development Tank

Aili Ting

Prepared by
Sandia National Laboratories
Albuquerque, New Mexico 87185 and Livermore, California 94550

Sandia is a multiprogram laboratory operated by Sandia Corporation, a Lockheed Martin Company, for the United States Department of Energy under Contract DE-AC04-94AL85000.

Issued by Sandia National Laboratories, operated for the United States Department of Energy by Sandia Corporation.

Available to DOE and DOE contractors from
U.S. Department of Energy
Office of Scientific and Technical Information
P.O. Box 62
Oak Ridge, TN 37831

Telephone: (865)576-8401
Facsimile: (865)576-5728
E-Mail: reports@adonis.osti.gov
Online ordering: http://www.doe.gov/bridge

Available to the public from
U.S. Department of Commerce
National Technical Information Service
5285 Port Royal Rd
Springfield, VA 22161

Telephone: (800)553-6847
Facsimile: (703)605-6900
E-Mail: orders@ntis.fedworld.gov
Online order: http://www.ntis.gov/ordering.htm

SAND2002-8333
Unlimited Release
Printed August 2002

Pressure Waves Induced by Megasonic Agitation in a LIGA Development Tank and Resist Feature Cavities

Aili Ting
Sandia National Laboratories
Livermore, California 94551-0969

ABSTRACT

Megasonic agitation is used to improve the uniformity of the LIGA[1] development process. To investigate the acoustic wave fields induced by megasonic agitation, we compute wave fields for a development tank containing a submerged wafer and for a typical trench-like feature on the wafer face. This separate treatment of these two problems is advantageous, because the length scales of the tank and the feature differ by three to four orders of magnitude.

A spectral method based on Green's functions is used to construct the acoustic wave field, avoiding the alternative of solving partial differential equations over the entire domain. The total acoustic wave field is obtained by superposing of the primary wave field and the first reflected wave field, which are computed in sequence without any need for iterations. The wafer interference to the wave field is treated directly by a priori recognition of shadow regions in the primary field and a concept of boundary of dependence in the reflected field.

Unlike a divergent wave field produced by ultrasonic agitation, results show that the wave field in the tank becomes narrowly focused at megasonic frequencies such that the most effective agitation is confined in a region directly above the acoustic source; this numerical expectation has been verified analytically and further confirmed experimentally by Sandia's LIGA Group.[13] The amplitude of the focused wave pressure is proportional to square root of the wave frequency. The wave pattern in a feature cavity also depends strongly on the orientation of the wafer and the aspect ratio of the cavity.

It is concluded that the LIGA development process will be greatly accelerated, if the orientation and the location of the immersed wafer is arranged so that the wafer spends more time in the focused wave field of high frequency agitation.

[1] LIGA (**Li**thographie, **G**alvanotormug, **A**bformung in German) means lithography, electroplating, and molding.

ACKNOWLEDGMENTS

The present work was funded by Materials and Physics Models Project of the Sandia Accelerated Strategic Computing Initiative. Sandia is a multiprogram laboratory operated by Sandia Corporation, a Lockheed Martin Company, for the United States Department of Energy under contract DE-AC04-94AL85000.

The author would like to thank R. H. Nilson of Sandia National Laboratories for his thoughtful discussion and help in editing. The author also thanks M. Bankert for reviewing the manuscript.

CONTENTS

Figures

In LIGA resist development, a wafer pre-exposed through a patterned mask is placed in a liquid chemical developer bath to dissolve the exposed regions. The resulting nonconducting mold is then filled by electrodeposition to produce metal microstructures. The features of these structures typically have lateral dimensions on the order of 10–1000 microns, and the aspect ratio of feature depth to feature width can be as high as 100. Thus, transport of dissolved polymer fragments from the feature bottoms often controls the rate of development. Slender feature cavities generally require long development times, because the fluid inside these cavities is almost stagnant,[1] while the large better-circulated feature cavities require much shorter times. Therefore, while a narrow cavity still remains underdeveloped, a wide cavity may often be overdeveloped causing unwanted sidewall taper in regions under the exposure mask and undercutting at the bottom corners in regions subjected to substrate emission (see Figure 1). A slender post with wide cavities on both sides may even be detached from the substrate by undercutting. Thus, the process not only is very slow but also may lead to unacceptable uniformity, even with the help of stirring or low frequency agitation of the bulk fluid.

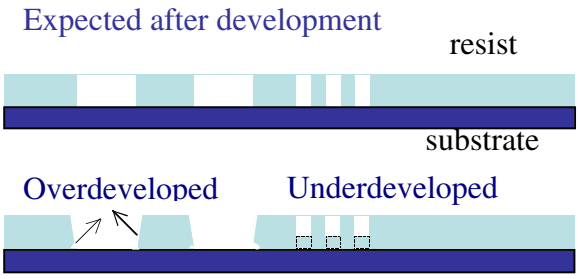

Figure 1. Over- and Under-Development

High-frequency acoustic agitation, or megasonic agitation, whose frequency ranges from about 0.7 to 2 MHz, is known to enhance the development process. To produce the high-frequency acoustic waves, a series of transducers are installed at the bottom of the development tank with each transducer strip being activated in sequence. The width of each strip is much smaller than that of the tank.

Megasonic waves, generated by the transducers propagate upward, oscillate the fluid and accelerate the development process. Previous studies of acoustic agitation in LIGA development and other lithographic applications show that agitation can achieve a more stable development process, enhance development uniformity, increase the development

rate, shorten the development time, increase the effective sensitivity, and lower the effective exposure energy.[2-5] The Sandia LIGA group currently uses a PCT Megasonic Cleaning Tank[6] to do their LIGA development. The high-frequency waves with high acoustic energy (10-30 W/cm^2) not only enhances fluid transport into slender feature cavities, but may also increase surface dissolution kinetics, increase surface activities, improve wetting efficiency (reduce surface tension), and prevent the formation of large bubbles that could damage resist fragile features.[6] Figure 2 shows the sketch of a pre-exposed wafer immersed in the liquid developer tank equipped with acoustic agitation transducers.

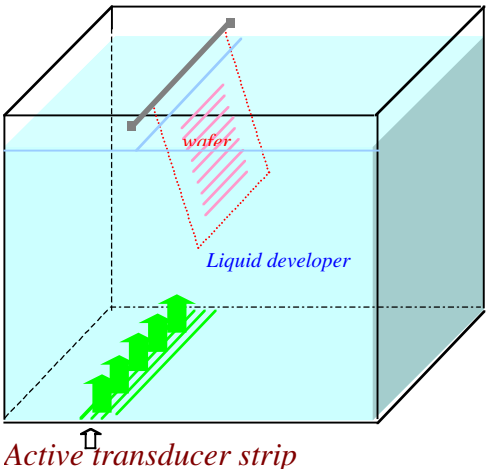

Figure 2. Sketch of a LIGA Development Tank

To understand how acoustic waves enhance the development process, there are two separate problems to solve: the tank-scale problem and the feature-scale problem. The reason for this separate treatment is that the length scales of two problems are several orders of magnitudeapart, from centimeters to microns. At the tank-scale, the wafer may be viewed as a flat surface without any attention paid to surface details. The results of the tank-scale problem reveal the acoustic wave pattern and acoustic energy distribution inside the tank and at the wafer surface, resulting from the interaction of the waves generated by the transducer and those reflected from the tank and from the wafer. The pressure distribution on the wafer surface provides boundary conditions for solving the feature-scale problem. The detailed analysis of a single feature reveals the wave pattern, pressure distribution, and first order fluid motion within a typical cavity. The results from both problems help us to identify the best wafer orientation in the tank, to shorten substantially the development time and to improve uniformity.

Spectral, or Green's function, methods are often used to solve wave problems. The great advantage of this approach is that the solution is constructed by integration of Green's Identity over the boundary elements. There is no need to solve the partial differential

equation on the interior of the domain or to treat the singularities and degenerated matrices as in FEM and BEM methods. In addition, a much finer grid and higher resolution can be achieved than in finite element or boundary integral methods. For example, the commercial software package, SYSNOISE,[7] is only able to compute large-scale wave problems for wave frequencies up to 300 kHz, much smaller than megasonic, while we can easily reach 1 MHz waves without losing accuracy.

The total acoustic wave field is obtained by superposition of the primary wave field and the first reflected wave field, which are computed in sequence following a method used by German authors S, Dahnke and F. J. Keil,[8] to treate a three-dimensional tank. Although their analysis included the formation of acoustic bubbles, there was no wafer within the tank. However, a challenging aspect of the present work is to treat the interference of the wafer with the primary and the reflected wave fields. We have tried several approaches such as iteration between waves in a tank without a wafer and a wafer in an infinite wave field, and iteration between two regions in the tank divided by the wafer, but neither of these was successful. Finally, we developed a new direct approach using a priori knowledge of shadow region in the primary wave field and the boundary of dependence in the reflected wave field to treat wave interactions with the wafer, avoiding any iteration.

In the following sections, we present the boundary value problem of acoustic waves, the spectral method for solving wave problems, the decomposition into primary and secondary wave fields, the concepts of shadow regions and boundaries of dependence, and examples of tank-scale and feature-scale solutions.

BOUNDARY VALUE PROBLEM OF ACOUSTIC WAVES

The hyperbolic partial differential wave equation $c_0^2 \nabla^2 \Phi = \partial^2 \Phi / \partial t^2$ describes the general behavior of non-dispersed waves in an inviscid fluid, where c_0 is the wave speed in the fluid, and Φ is the velocity potential function of the fluid, ($\boldsymbol{u} = \nabla \Phi$, where $\boldsymbol{u}$ is a velocity vector). The function $e^{i\omega t}$ describes the time dependence of the periodic wave motion, where $i^2 = -1$, ω is the wave angular frequency ($\omega = kc_0$), a constant frequency for non-dispersed waves, and k is wave number. The reduced potential function, ϕ, is related to

the velocity potential function as $\phi = \Phi e^{-i\omega t}$, and thus satisfies the elliptic Helmholtz equation, $\nabla^2\phi + k^2\phi = 0$.

The wave induced pressure and density changes are defined as: $p_{\text{wave}} = p - p_0$, $\rho_{\text{wave}} = \rho - \rho_0$ where p and ρ are the total pressure and total density in the fluid, respectively; p_0 and ρ_0 are the undisturbed constant pressure and density, respectively. Both p_{wave} and ρ_{wave} range between positive and negative values, superposed on their undisturbed values to obtain the total quantities. The velocity field in the fluid, $\boldsymbol{u}$, is induced purely by the acoustic waves. From Euler's momentum equation for invisid flow, it follows,

$$\rho\partial\boldsymbol{u}/\partial t + \rho(\boldsymbol{u}\bullet\nabla)\boldsymbol{u} = -\nabla p, \qquad \nabla\times\boldsymbol{u} = 0 \Rightarrow \boldsymbol{u} = \nabla\Phi,$$
$$(\boldsymbol{u}\bullet\nabla)\boldsymbol{u} = \nabla(\boldsymbol{u}^2/2) - \boldsymbol{u}\times(\nabla\times\boldsymbol{u}) = \nabla(\boldsymbol{u}^2/2)$$
$$(\rho_0 + \rho_{\text{wave}})\nabla(\partial\Phi/\partial t + \boldsymbol{u}^2/2) + \nabla p = 0,$$
$$\nabla[\rho_0(\partial\Phi/\partial t + \boldsymbol{u}^2/2)] + \nabla p = 0,$$

where ∇ and $\times$ are gradient operator and vector product operator, respectively. The wave-induced fluid density change is very small compared to the undisturbed fluid density especially for a liquid, $\rho_{\text{wave}} \ll \rho_0$. Thus, in the above equations, ρ_{wave} can be neglected compared to ρ_0, and ρ_0 can be moved under the ∇ operator. Then, by integrating the last equation, and selecting the integration constant at the free surface,

$$\rho_0(\partial\Phi/\partial t + \boldsymbol{u}^2/2) + p = p_0 + \rho_0(\boldsymbol{u}^2/2)_{\text{free surface}}$$
$$p_{\text{wave}} = -\rho_0[\partial\Phi/\partial t + \boldsymbol{u}^2/2 - (\boldsymbol{u}^2/2)_{\text{free surface}}]$$
$$\Rightarrow p_{\text{wave}} \approx -\rho_0\partial\Phi/\partial t = -i\rho_0\omega\phi.$$

A linear approximation is obtained by neglecting the nonlinear dynamic pressure difference, $-\rho_0[\boldsymbol{u}^2/2 - (\boldsymbol{u}^2/2)_{\text{free surface}}]$, which is generally much smaller than the linear time dependent term. In fact, the transient term can be estimated as $\partial\Phi/\partial t \sim |\boldsymbol{u}|c_0$ because of $|\Phi| \sim |\boldsymbol{u}|\lambda$, so by comparing the order of magnitudes between the transient pressure term and the dynamic pressure term, it follows that $(\boldsymbol{u}^2/2) / (\partial\Phi/\partial t) \sim |\boldsymbol{u}| / 2c_0 \ll 1$. Under this simplification, the first order wave pressure is entirely due to the time dependent term that is proportional to the reduced potential function and the wave frequency. In addition, the expression for the wave speed, $c_0^2 = (dp/d\rho)_s$ (where s is entropy), becomes

equal to $|p_{wave}| / |\rho_{wave}|$, indicating that the amplitude of p_{wave} is c_0^2 times larger than the amplitude of ρ_{wave}—six orders of magnitude larger in our application since c_0 is 1500 m/s. Thus, the wave pressure, p_{wave}, in contrast to the wave density, ρ_{wave}, is not necessarily small compared to the undisturbed pressure, p_0. For megahertz frequencies and typical acoustic bath intensities p_{wave} can be two or three atmospheres. From the above expressions it can also be seen that the wave pressure p_{wave} satisfies the Helmholtz equation and that the fluid velocity vector, $\boldsymbol{u}$, is proportional to the gradient of wave pressure, ∇p_{wave}.

The typical boundary conditions for the reduced potential function, ϕ, are the Neumann and Dirichlet conditions. A zero normal velocity or no flux condition, $\partial\phi/\partial n = 0$, is applied on all solid walls. A prescribed upward periodic velocity, $\partial\phi/\partial n = -u_0.e^{i\omega t}$, is applied at the surface of a transducer strip, and a constant total pressure or zero wave pressure, that is $\phi = 0$, is applied on the free surface of the tank problem.

Physically, acoustic waves generated by the transducers on the tank bottom are reflected from all tank walls, both wafer surfaces, and the free surface. However, there is an essential difference between wall reflection and free surface reflection. At a high impedance wall, the incoming wave and reflected waves satisfy an optical reflection law, such that the wave pressure at the wall is doubled. At a free surface, a pressure release boundary condition (static pressure or a zero wave pressure) indicates the cancellation between the incoming and reflected waves. Here, the reflected wave has a phase difference of π from the incoming wave.

A Spectral Green's Function Method for Solving Wave Problems

The Green's functions of Helmholtz equations are spherical and cylindrical waves of variable frequency. [9-10] The Green's function approach we adopted is a direct method for solving wave problems.

Spherical and Cylindrical Waves from Helmholtz Equation

The free space Green's function G for a three-dimensional Helmholtz equation is the spherical wave. It satisfies the equation

$$\nabla^2 G(x, y, z; x', y', z') + k^2 G(x, y, z; x', y', z') = \delta(x - x', y - y', z - z').$$

$$G(x, y, z; x', y', z') = -\frac{e^{-ikR}}{4\pi R},$$

where (x, y, z) and (x', y', z') describe the locations of field points and acoustic source points, respectively; $R = [(x - x')^2 + (y - y')^2 + (z - z')^2]^{1/2}$, δ is the Dirac delta function.

Similarly, the free space Green's function G_2 for a two-dimensional Helmholtz equation is a cylindrical wave; it can be obtained by natural extension of spherical waves. For example, a three-dimensional tank problem may be reduced to a two-dimensional problem in which the acoustic source is an infinitely long strip source of finite width. Integration the spherical free-space Green's function G along the y′ axis from -∞ to +∞ yields a free-space cylindrical wave function G_2.[9] G_2 is proportional to a zero-order Hankel function of the second kind— a complex function in the Bessel function family.[11]

$$G_2(x, y; z, z') = \int_{-\infty}^{\infty} G(x, y, z; x', y', z')dy' = -\frac{1}{4\pi}\int_{-\infty}^{\infty} \frac{e^{-ik\sqrt{r^2 + (y-y')^2}}}{\sqrt{r^2 + (y-y')^2}} dy'$$

$$= -\frac{1}{2\pi}\int_{o}^{\infty} \frac{e^{-ikr\sqrt{1+t^2}}}{\sqrt{1+t^2}} dt = \frac{i}{4} H_o^{(2)}(kr)$$

where $t = (y' - y)/r$, $r = [(x - x')^2 + (z - z')^2]^{1/2}$

Potential Function and The Green's Identity

The well-known Green's Identity can be used to construct solutions of the Helmholtz equation based on boundary information. It indicates that an elliptical potential function, $\phi(x, y, z)$, within an enclosure is determined uniquely by the values of the Green's function G, potential function ϕ, and both of their outward normal derivatives at the enclosure surface provided that G and ϕ are differentiable inside the region and at the boundary S.

$$\alpha\,\phi(x, y, z) = \oint_S (\phi\nabla' G - G\nabla'\phi)\bullet \boldsymbol{n} ds$$

$\alpha = \sigma/4\pi$ or $\sigma/2\pi$,	for three- and two-dimensional case, respectively.
$\alpha = 1$,	(x, y, z) inside the region, since $\sigma = 2\pi$ or 4π.
$\alpha = 0$,	(x, y, z) outside of region, since $\sigma = 0$.
$0 < \alpha < 1$,	(x, y, z) at boundary.

where α is a parameter, σ is solid angle[2] from point (x, y, z) to enclosure boundary S, $\boldsymbol{n}$ is the unit outer-normal vector to S, and the gradient operator, ∇', is taken at x', y', z'. Thus, to obtain the potential function at a field point, the values of the Green's function, the potential function, ϕ, which represents pressure, and their normal derivatives, $\partial\phi/\partial n$, which represents normal velocity, are needed on all bounding surfaces. According to the present boundary conditions, Green's integral has a nonzero first term, $\phi\,\partial G/\partial n$, only on a solid wall and a nonzero second term, $G\partial\phi/\partial n$, only on a free surface, but these values of ϕ at each wall and $\partial\phi/\partial n$ at the free surface are not known a priori. To overcome this difficulty we will split the solution into primary and secondary components that together satisfy all of the boundary conditions. As explained immediately below, the primary wave field driven by the acoustic transducers is constructed first using only conditions on the tank floor. The boundary conditions on all other surfaces are later satisfied through construction of the secondary wave field.

Primary Wave field and Half Space Green's Function

Suppose that the acoustic source is distributed on a part s_1 (here, the transducer surface) of the $z' = 0$ plane, while the rest of $z' = 0$ is *a* solid wall or rigid baffle. The Green's function for this half-space geometry can be constructed from two equal-strength spherical sources located at $(x', y', \pm z')$ as $z' \to 0$. Then the primary field can be found by the Green's identity of this half-space Green' function, in which the integration is needed only on the transducer surface.

This new Green's function is

$$G(x,y,z;x',y',z') = -\frac{e^{-ikR_1}}{4\pi R_1} - \frac{e^{-ikR_2}}{4\pi R_2}$$

$$R_1 = \sqrt{(x-x')^2 + (y-y')^2 + (z-z')^2}$$

$$R_2 = \sqrt{(x-x')^2 + (y-y')^2 + (z+z')^2}$$

[2] In fact, $\sigma = -\int_s \nabla'(1/R)\bullet\boldsymbol{n} ds$ and $\sigma = \int_s \nabla'(\ln r)\bullet\boldsymbol{n} dl$ are the solid angles in three- and two-dimensional cases, respectively, for any S. They can easily be seen when S is a spherical surface or a circle.

The normal derivative of this Green's function with respect to z' will not be zero at any field point location z for source location with $z' \neq 0$. Only when the vertical distance between these two sources vanishes, $z' \to 0$, $R_1 = R_2 = R$, the two sources form a new source on the symmetry plane $z' = 0$ such that the normal derivative is zero in this plane of symmetry. This is defined as the half space Green's function G_h because it satisfies the half space boundary condition, $\partial G_h/\partial z' = 0$ at $z' = 0$.

$$G(x,y,z;x',y',0) \to G_h(x,y,z;x',y',0) = -\frac{1}{2\pi}\frac{e^{-ikR}}{R},$$

$$R = \sqrt{(x-x')^2 + (y-y')^2 + z^2}\ , \quad \frac{\partial G_h}{\partial z'}\Big|_{z'=0} = 0$$

Similarly, the half-space Green's function for the two-dimensional Helmholtz equation is

$$G_2(x,z;x',0) \to G_{2h}(x,z;x',0) = -\frac{i}{2}H_0^{(2)}(kr),$$

$$r = \sqrt{(x-x')^2 + z^2} \qquad \frac{\partial G_{2h}}{\partial z'}\Big|_{z'=0} = 0$$

When applying this half–space Green's function to Green's Identity, the enclosure surface includes $z = 0$ and a far-field surface extended to infinity, whereon ϕ and its normal derivative vanish due to the very large distance R from the source. In fact, the far-field surface can be considered a half-spherical surface of R, and then the integration will become: $2\pi R^2 G\,[\partial\phi/\partial R - (1/R + ik)\phi] \approx (e^{-ikR}/2)[R\,(\partial\phi/\partial R + ik\phi)] \to 0$ as $R \to \infty$. The expression $R\,(\partial\phi/\partial R + ik\phi) \to 0$ as $R \to \infty$ is just the far-field Sommerfeld radiation condition. Under this condition, Green's integral is nonzero on only the transducer surface, s_1, because $\partial\phi/\partial n$ is zero on all other portions of $z = 0$. Thus, if an acoustic source is distributed on a planar surface $s_1(x', y', z') = 0$, the potential function will be

$$\phi(x,y,z) = -\int_{s_1} G_h(x,y,z;x',y',z')\nabla'\phi(x',y',z')\bullet \boldsymbol{n}(x',y',z')ds$$

$$= -\frac{u_0}{2\pi}\int_{s_1}\frac{e^{-ikR}}{R}ds \qquad u_0 = -\frac{\partial\phi}{\partial n}\Big|_{s_1}$$

The last of these expressions applies to a flat piston transducer surround by a rigid baffle, where u_0 is the transducer velocity normal to the surface. Note that if u_0 is position dependent, it should be placed inside the integral. Similarly, the two-dimensional far-field Sommerfeld radiation condition, $r^{1/2}\,[\partial\phi/\partial r + ik\phi] \to 0$ as $r \to \infty$ (due to $H_0^{(2)}(kr) \to (2/\pi kr)^{1/2}e^{-i(kr-\pi/4)}$) makes the far field integration vanish, so the reduced potential function ϕ_2 for a half-space problem satisfies the following equation

$$\phi_2(x,z) = -\int_{s_1} G_{2h}(x,z;x',0)\nabla'\phi_2(x',z')\bullet \boldsymbol{n}(x',z')ds$$

$$= -\frac{iu_0}{2}\int_{s_1} H_0^{(2)}[k\sqrt{(x-x')^2+z^2}]ds \qquad u_0 = -\frac{\partial\phi}{\partial n}\Big|_{s_1}$$

in which $s_1(x', y')=0$ is the planar surface containing the acoustic source. This expression is used in this work to construct the two-dimensional primary wave field without considering wave reflections.

If the known boundary condition at a flat piston transducer is pressure instead of velocity, the appropriate half-space Green's function can be derived by combining a pair of free-space Green's functions having equal strengths but opposite signs. It follows that

$$G(x,y,z;x',y',z') = -\frac{e^{-ikR_1}}{4\pi R_1} + \frac{e^{-ikR_2}}{4\pi R_2}$$

as $z' \to 0$: $G(x, y, z; x', y', 0) \to G_h(x, y, z; x', y', 0) = 0$,

$\partial G_h/\partial z' \neq 0$ at symmetry plane $z' = 0$,

$$\phi(x,y,z) = \int_{s_1} \phi(x',y',z')\nabla' G_h(x,y,z;x',y',z')\bullet \boldsymbol{n}(x',y',z')ds$$

$$= \frac{i}{4\pi\rho\omega}\int_{s_1} p_t \nabla[\frac{e^{-ikR}}{R}]\bullet \boldsymbol{n}ds$$

where p_t is the known pressure at the acoustic source (transducer surface). Similarly, in the two-dimensional case,

as $z' \to 0$: $G_2(x, z; x', 0) \to G_{2h}(x, z; x', 0) = 0$,

$\partial G_{2h}/\partial z' \neq 0$ at symmetry plane $z' = 0$,

$$\phi_2(x,z) = \int_{s_1} \phi_2(x',z')\nabla' G_{2h}(x,z;x',z')\bullet \boldsymbol{n}(x',z')ds$$

$$= \frac{1}{4\rho\omega}\int_{s_1} p_t \nabla[H_0^{(2)}(kr)]\bullet \boldsymbol{n}ds$$

All of the preceding half-space Green's functions provide relatively simple descriptions of the primary wave field as well as the information (incident ϕ or $\partial\phi/\partial n$) needed to compute wave reflections from the boundaries.

Reflected Wave field and Free Space Green's Function

The primary waves of the preceding section are reflected at all boundaries to produce secondary waves. The sum of these two fields, primary and reflected, will be used here to represent the total wave field with the understanding that higher-order reflections may also contribute, particularly in narrow enclosures where divergence effects are small. Knowledge of the incident primary wave field on each boundary provides all the

information needed to compute the secondary field from the free-space Green's function and Green's Identity.

$$\phi = \oint_S [\phi \frac{\partial G}{\partial n} - G \frac{\partial \phi}{\partial n}] ds$$

where G is the free space Green's function, and S is the entire enclosure boundary including every wall and free surface. Note that in the two dimensional case, $\phi = \phi_2$, and $G = G_2$.

Boundary Value Problems for Primary and Reflected Acoustic Waves

Let the reduced potential function ϕ be the summation of the primary field, ϕ_P, and the reflected field, ϕ_R. The boundary conditions for each of these components are determined by the boundary conditions for the total field and by the reflective properties of the surface. The resulting boundary value problems may thus be described as follows:
Helmholtz equation,

$$\nabla^2 \phi + k^2 \phi = 0$$

where $\phi = \phi_P + \phi_R$

At a rigid wall,

$$\frac{\partial \phi}{\partial n} = \frac{\partial \phi_P}{\partial n} + \frac{\partial \phi_R}{\partial n} = 0$$

$$\frac{\partial \phi_R}{\partial n} = -\frac{\partial \phi_P}{\partial n}$$

$$\phi = 2\phi_P, \qquad \phi_P = \phi_R$$

Since there is assumed to be no displacement at these rigid walls, the normal velocity of reflected wave just offsets the normal velocity induced by the primary wave field. Since the waves have equal magnitudes but opposite signs, the pressure of the reflected wave is equal to the pressure of the primary wave, so the resulting total pressure is twice the incident pressure. In the special case of the tank bottom, there is no first reflection because the spherical or cylindrical wave beams emitted from the source are coincident with the bottom surface.

At a free surface, $\phi = 0 \qquad \phi_P = -\phi_R$

$$\frac{\partial \phi}{\partial n} = \frac{\partial \phi_P}{\partial n} + \frac{\partial \phi_R}{\partial n} = 2\frac{\partial \phi_P}{\partial n}$$

$$\frac{\partial \phi_R}{\partial n} = +\frac{\partial \phi_P}{\partial n}$$

At the free surface, the total pressure in the bath liquid must always remain equal to the ambient atmospheric pressure. Because of the anti-symmetry of the reflection law, the equal but opposite wave pressures cancel each other and produce a doubling of the fluid velocity.

In summary, the primary wave field and the first reflected wave field are constructed sequentially using Green's identity. The half-space Green's function is first used to construct the primary field driven by the transducer. These results, the boundary conditions at reflective surfaces, and the free-space Green's function are then used to construct the reflected field. In this manner all of the boundary conditions are satisfied without any need for iteration. This approach avoids the necessity of solving a large and often ill-posed set of simultaneous algebraic equations in a conventional BEM.

Procedure For Solving Primary and Reflected Wave Fields

The computational procedure is straightforward. First, we calculate the primary wave field ϕ_P excited by the transducer surface using the half-space Green's function. At each of the interior or boundary points of interest, we replace the Green's integral representation by a summation over a series of discrete elements representing the surface of the acoustic driver. Second, we use computed values of the primary field and its values on the boundary surfaces to set up boundary conditions for the first reflected wave field ϕ_R on all walls and free surfaces (only for tank problem). Third, calculate the reflected wave field ϕ_R using the free-space Green's function. In this calculation, the Green's integral representation is replaced by a summation over all of the discrete elements on all reflective and or free surfaces. Finally, calculate the total wave field by summation of the primary and reflected wave fields. This summation need only be performed at points of interest, such as the front wafer face. However, in the present test calculations we have computed the wave field throughout the interior.

In this work, the second reflected wave field and beyond are all neglected, assuming they are considerably weaker than the first reflected field. Nevertheless, the second reflections can be calculated in the same way as the first. In doing this, the first reflections become the incident waves to be cancelled or doubled by the second reflections at the boundary surfaces, and so on. Since these wave fields generally become sequentially weaker, owing mainly to divergence effects, only the first reflection field are generally required, particularly if the region of interest lies in the central part of a relatively large cavity, as in the case of our submerged wafer.

ACOUSTIC WAVES IN A TWO DIMENSIONAL TANK WITH WAFER

For a frequency of around 1 MHz, the acoustic wavelength in the developer fluid (having water-like properties) is only about 1.5 mm, while the developer tank sketched in Figure 3 has a length scale of around 0.3 m. Thus, to obtain even a relatively sparse resolution of six nodal points per wavelength would require a grid having 1200^3 elements. To replace the computational burden, we chose to compute the wave field in a two-dimensional cross-section of the tank, as though each of the transducer strips was infinite in length. In the following sections, comparison with experimental data will show that the two dimensional results are sufficiently good that there is little need for complex three dimensional calculations.

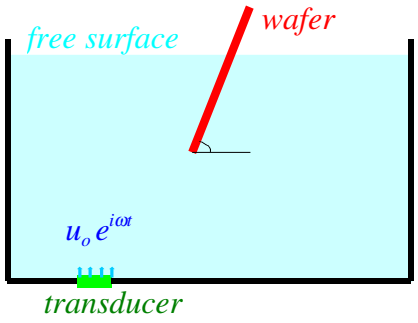

Figure 3. Two-Dimensional Tank

Interaction Between the Wafer and Acoustic Waves in the Tank

When the wafer is absent, the acoustic waves in the development tank can be readily computed using the described Green's function approach. This case also served as a convenient test problem, since the solution can also be constructed by summation of mirror images. It is difficult, however, to apply the mirror images technique when the wafer is present or the tank is three-dimensional.

The situation becomes complicated when the wafer is involved. Assuming that waves cannot penetrate the rigid wafer, they are fully reflected, doubling the pressure on all parts exposed to the primary field. Depending on the wafer orientation, the pressures on the opposing faces may be entirely different.

Shadow Region in Primary Wave Field

A shadow region is defined as any region that cannot be directly reached by primary wave beams. Without loss of generality we assume that the active transducer is on the left side of the tank and that the wafer is at an angle θ to the tank bottom. If the wafer is positioned at an angle greater then 90° clockwise from the tank bottom, there is a shadow region behind the wafer for wave beams emitted from each source point X' on the transducer (the left sketch in Figure 4). Similarly, if the wafer is at an angle less then 90°, there is a shadow region in front of the wafer for each source point X' on the transducer (the right sketch in Figure 4). These shadow regions can be reached only by reflected acoustic waves, not by primary waves.

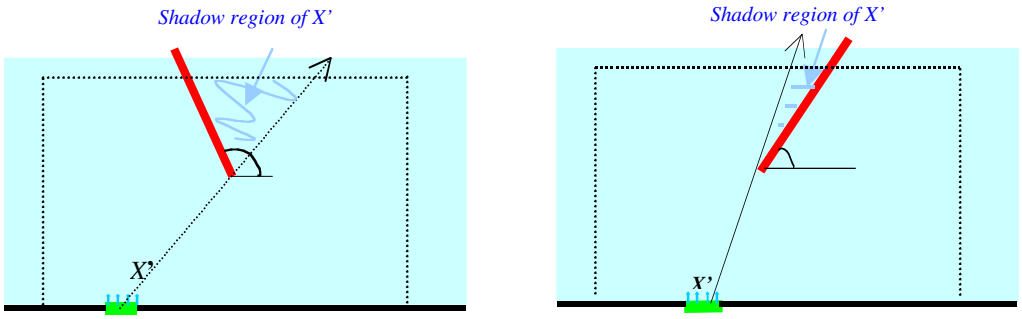

Figure 4 Shadow Region in Primary Field

Thus, when a wafer is present, the procedure for calculation of the primary wave field must take into account the presence of shadow region associated with each source point on the transducer.

Boundary of Dependence in Reflected Wave Field

Similarly, waves reflected from some boundary segments may not have a direct path to a field point under consideration. Thus, in summing the reflected wave contributions to Green's integral at a particular point, we include only those boundary segments having a direct line of sight. This collection of boundary segments, which may include wafer

surfaces, tank surfaces, and free surfaces, is referred to as the boundary of dependence. Obviously, only one side of the wafer can be seen by any field point. Figure 5 shows

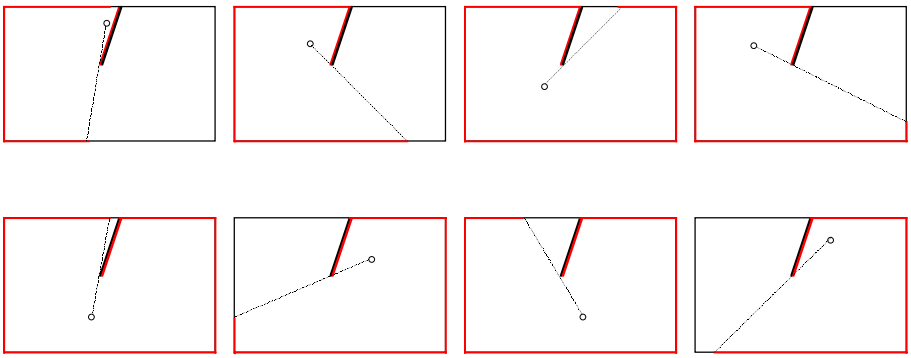

Figure 5. Boundary of Dependence (in red) in Reflected Field

several examples of the boundary of dependence. The solid angle from the field point intersects the boundary and determines the boundary of dependence (marked in red) for that field point. Only these boundary segments are included in the Green's integral summation of incoming reflected waves reaching the point under consideration.

Examples of High and Mid-Low Frequency Wave Fields

The dimension of the tank is 0.25 m × 0.20 m × 0.20 m. The magasonic agitation example has a wave frequency of f = 750 kHz, corresponding to a wave number, $k = (2\pi f / c_o) = 1000\ \pi\ (\text{m})^{-1}$, for a tank containing a liquid developer having a sound speed of c_o = 1500 m/s. Since the wavelength is $\lambda = c_o/f$ = 2 mm, with at least six nodes per wavelength, there are 750 × 600 + 300 = 450,300 nodes in the field and 3,300 boundary elements if the wafer has 300 × 300 nodes at each side. The one-inch acoustic source at the tank bottom represents an activated transducer strip. To enhance the resolution, Gaussian quadrature (n = 4) has been used in every interval of numerical integration. It took about 25–50 hours to complete a case on a SUN-ULTRA-2 workstation. The size of each of the resulting contour plot files describing the wave pattern in the tank can be as large as 66 megabytes.

For comparison, an example of mid-low wave frequency, 37.5 kHz, is also calculated. Since the wavelength is longer at lower frequencies, good resolution is obtained using100 nodes along each side of the tank and 50 nodes on each side of the wafer.

Mid-Low Frequency Examples

Compared to a few hundreds hertz, 37.5 kHz is a relatively high frequency; however, it is a mid-low frequency relative to megahertz. Figure 6 presents the pressure wave pattern in the tank without a wafer, resulting from the agitation at 37.5 kHz (wavelength 4 cm). The acoustic source is located at the tank bottom where the negative peak (in blue) can be seen in the first figure. The first three contour plots and the next three surface plots show the primary, reflected, and total wave fields, respectively. Since the height of the tank is 0.20 cm, five cylindrical waves of the primary field are spaced evenly from the tank bottom to the free surface with their peaks attenuated with range (in Figure 6a). As indicated in a later discussion section, the near wave field lies within about 0.64 cm off the acoustic source, so most of the wave field of interest may be viewed as the far field.

In the reflected and total fields, again five waves can be identified. Reflection at the right sidewall far from the source is weak. The strong reflection from the free surface interacting with the reflections from both sidewall results in multiple peaks in each wave front. The total field, which is a summation of the primary and the reflected fields, is not everywhere stronger than the primary field due to some wave cancellations. The total field remains strong at its multiple peaks, especially at the upper left corner due to the overlap of reflections from the free surface and the left sidewall.

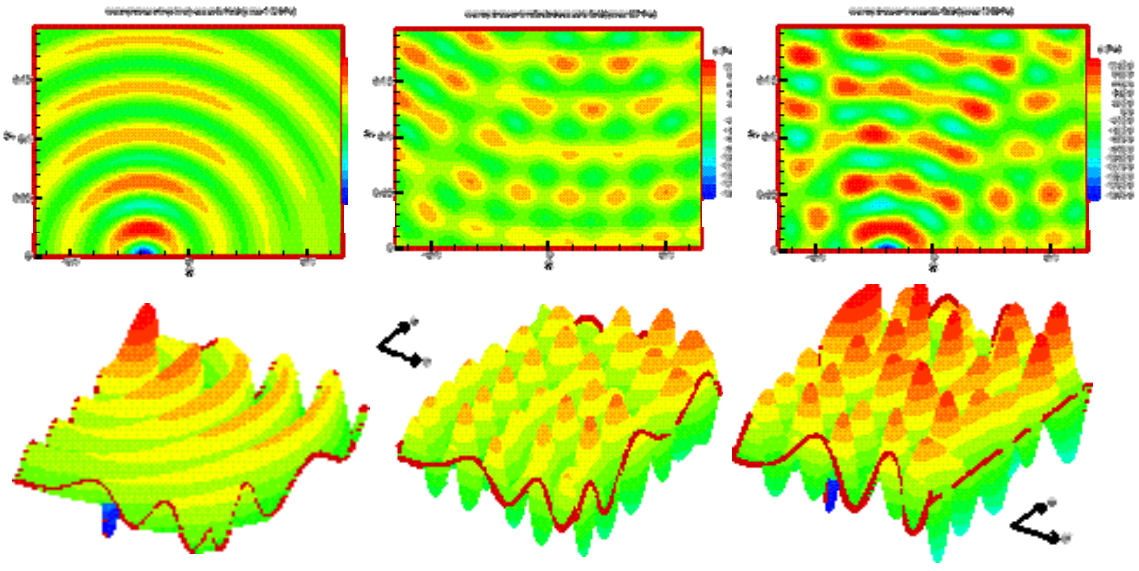

Figure 6. Primary, Reflected and Total Acoustic Wave Fields (left to right) in a Tank without a Wafer. (f =37.5 kHz, u_0 = 0.001 m/s, source located at –0.065 to –0.039 m)

From the three surface plots in which the tank bottom is the upper left boundary, the peaks are clearly seen, and the waves at the right sidewall (lower left boundary) and the free surface (lower right boundary) are obvious. Comparing these three surface plots, it is seen that the sidewall pressure of the primary field is equal exactly to that of the reflected field, doubling the pressure of the total wave field. Similarly, boundary conditions at the free surface shows that the primary wave pressure is exactly equal but opposite to the reflected wave pressure, making the zero pressure wave of total field.

The amplitude of the wave pressure is proportional to the magnitude of the source disturbance velocity u_0. As seen in the total field, the third contour or the third surface plot of Figure 6, the maximum rms wave pressure near the bottom source is 872 Pa while the rms pressure near the upper left corner is 540 Pa for $u_0 = 0.001$ m/s, and they will be 1.7 atm and 1.07 atm for $u_0 = 0.2$ m/s, respectively, which is estimated as the normal operation condition at a power input of about 6 W/m^2.[1] Therefore, even for agitation at mid-low frequency, the pressure disturbance can be more than atmospheric pressure (the total peak pressure will be more than 2 atm) at this operation condition. Thus, it can be expected that very high wave pressure will be achieved in high frequency agitation.

Figure 7 presents contour plots of the pressure wave pattern surrounding a wafer immersed in a tank with all other conditions the same as in Figure 6. The primary wave field has a shadow region that cannot be reached by direct wave beams. The reflected wave field is strong at the left upper half of the tank because of the interaction among reflected waves from the free surface, wafer and from the left sidewall. The shadow region of the primary field is filled with weak waves reflected from the right sidewall and from the free surface. Compared to the case having no wafer, the maximum total wave pressure is no stronger, but the waves amplitude is greater in the left half of the tank. Obviously, the left surface of the wafer that faces the acoustic source will get substantial agitation, but the right surface will not.

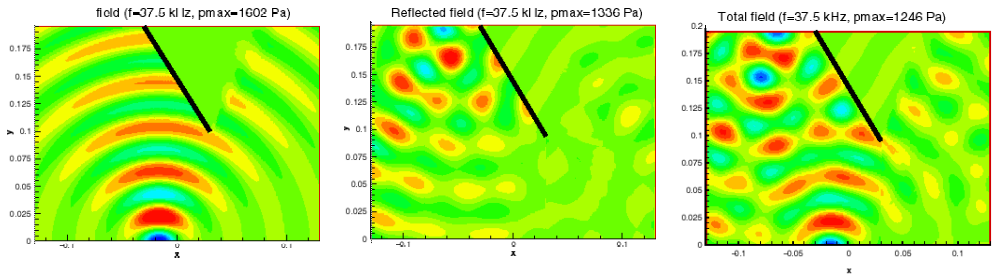

Figure 7. Primary, Reflected and Total Acoustic Wave Fields in a Tank containing a Wafer. (f =37.5 kHz, u_0 = 0.001 m/s, source located at –0.065 to –0.039 m)

High Frequency Examples

Figure 8 presents contour plots of the primary, reflected, and total wave fields for the 750 kHz case (without wafer). To our surprise, wave peaks are focused in a narrow region just above the acoustic source in all three fields. In the primary field, 100 waves are spread from the tank bottom to the free surface. Even at the one-inch width of the source, twelve waves are generated, which can also be identified at the far side of the surface plot (figure 9). Multiple waves in a row (twelve thin waves) are generated from the source (near field is within 0.32 mm, discussed later). When propagating upward, these very narrow waves interact with each other (transition region) and merge rapidly into a singles, wider wave (far field), which maintains a single-peak form with only minor divergence up to the free surface. This is a distinguishing feature of the high frequency waves; a wave train forms just above the source and propagates almost without divergence or decay. Outside of this wave train, there are many cylindrical wave beam rays expanding outward from the source in all directions but with substantially less intensity; there can also be seen in the surface plot.

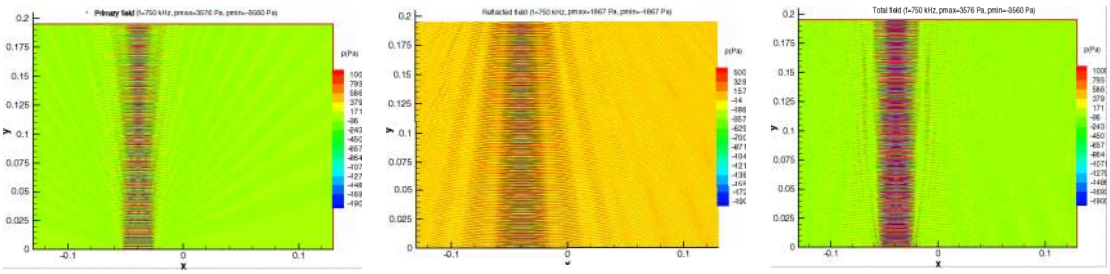

Figure 8. Primary, Reflected, and Total Acoustic Wave Fields in a Tank without a Wafer
(f=750 kHz, u_0 = 0.001 m/s, source located at –0.065 to –0.039 m)

The reflected field plot in the center of Figure 8 indicates that the major reflection is occurring at the free surface due to the local doubling of velocity. The colors in the reflected field have been adjusted by lowering the maximum contour values by one half to show more clearly the reflections from the free surface. The total field has a uniform wave train and is not very much stronger than the primary field due to the waves cancellation. There are secondary waves at both sides of the wave train, which can be seen in figure 9 (orientation different from contour plot, tank bottom is at the upper left). Here, as in Figure 8, multiple waves of narrow breath are emitted from the source and rapidly merge to form a wave train does not decay with range as in the mid-low frequency case. The surface plot also shows the much weaker waves outside the wave train, weak group-waves at the sidewall boundary, and zero wave pressure at the free surface.

For convenience, all of the preceding calculations are based on a velocity, u_0, of 1 mm/s, at the transducer surface. The corresponding maximum pressure of the total field is about $\langle p \rangle = p_{rms} = 0.5\ (pp^*)^{1/2} = 1458$ Pa. Here $\langle\rangle$ denotes the time average quantity, power intensity $I = \langle pu \rangle = \langle p \rangle^2 / (\rho c) = 0.000142$ W/cm^2, and p^* is the conjugate *of p.* At the plane 5 inches below the free surface where waves have not merged completely, the wave train pressure $p_{rms} = 1135$ Pa, I = 0.000086 W/cm^2. These conditions can be readily scaled to the any LIGA conditions of interest, as explained later.

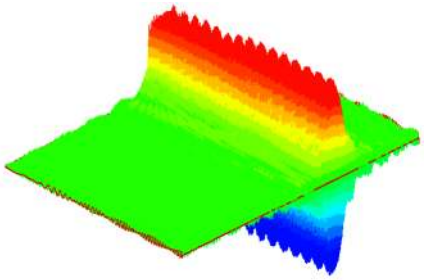

Figure 9. Surface Plot of Total Field

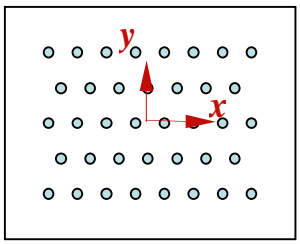

Figure 10. Measured Points in Horizontal Plane

Comparison with Experimental Data

Acoustic power intensity[12] inside a LIGA development tank (without a wafer) were measured by D. Larsen and M. Bankert[13]. The power intensity, *I*, is proportional to the square of the rms wave pressure. The measured positions generally include several locations along five rows in a particular horizontal plane, as shown in Figure 10. The

measured data for a depth of 5 inches below the liquid surface are presented in the Figure 11 for acoustic agitation by the first transducer strip at a frequency ranging from 646 to 694 kHz. These plots clearly show the narrow focusing of energy just above the activated first transducer strip, in agreement with the simulation. The peak power intensity is about 200 W/in^2 or 31 W/cm^2, which implies a rms peak wave pressure of about 6.73 atm and wave velocity of about 0.45 m/s, while the average power intensity in the tank is about 50 W / in^2 or 7.75 W/cm^2, which implies an average rms wave pressure of 3.365 atm and an average wave velocity of 0.225 m/s. This 7.75 W/cm^2 is just the average power intensity in typical LIGA application conditions.

The data describing the average, the maximum and the minimum from all five rows overlap into three single curves, indicating the data are nearly insensitive to the location in *Y*-direction. Therefore, the two-dimensional simulations appear to be quite adequate for present purposes, and there is no need to perform more complex three-dimensional calculations.

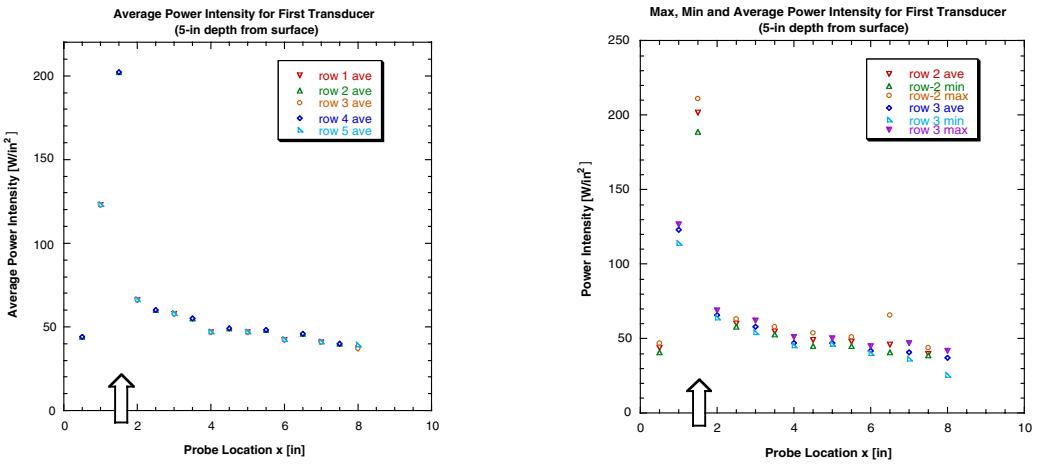

Figure 11. Measured Average (left), Max and Min (right) Power Intensities
For First Transducer at 5 in. deep from Surface.

Using the asymptotic expression based on the reduce potential in the Discussion 2 section, the velocity at the transducer surface should be around u_0 = 0.32 m/s for 7.75 W/cm^2. In this case, the max rms pressure of the total field at the plane 5 inches below the free surface becomes 1134.58 * 320 /101325 = 3.58 atm, and the average power density becomes 8.79 W/cm^2, while the absolute peak pressure and the power intensity at the

point will be 6.42 atm and 28 W/cm^2, respectively. These data are close to the measured data.

High Frequency Examples with a Wafer

Figure 12 presents the contour plots of the primary, reflected, and total wave fields when a wafer is immersed in the tank with all other conditions the same as in Figure 8. Primary acoustic waves impinge upon the left surface of the wafer, while the back face lies with a shadow region. The reflected wave field is again strong at the left upper half of the tank because of the interaction among reflected waves from the free surface, the wafer, and the left sidewall. The waves reflected from the sidewalls are too weak to see except at the upper right corner where some waves reflected from the free surface and from the right sidewall can be identified. Compared to the case without wafer, the maximum total wave

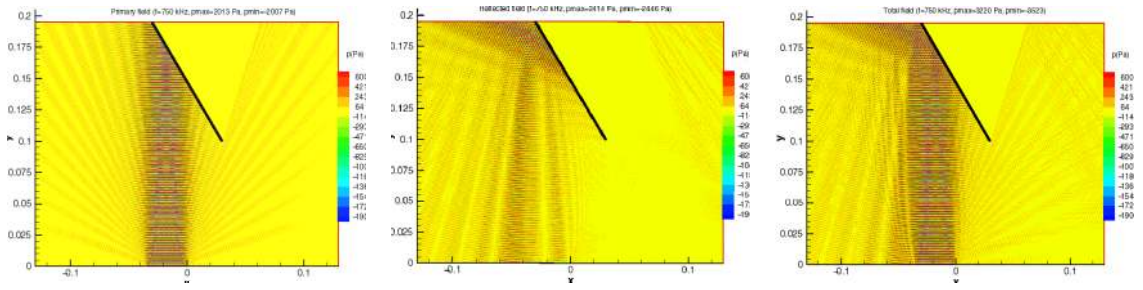

Figure 12. Primary, Reflected and Total Acoustic Wave Fields in a Tank with Wafer.
(f =750 kHz, u_0 = 0.001 m/s, source located at –0.065 to –0.039 m)

pressure is not necessarily stronger, except in the left upper quarter due to the wafer. Again, the left surface of the wafer facing the acoustic source will get much more agitation than the right surface and this agitation is much stronger than in mid-low frequency case.

Figure 13 depicts the total field for a case in which wafer does not interact directly with the primary wave train due to its orientation. In this case, there is no substantial agitation on either wafer face, even though the maximum pressure is at the same level as in Figure 8. Only a narrow triangular region at the left end of the wafer surface is filled by relatively weak waves reflected from the free surface.

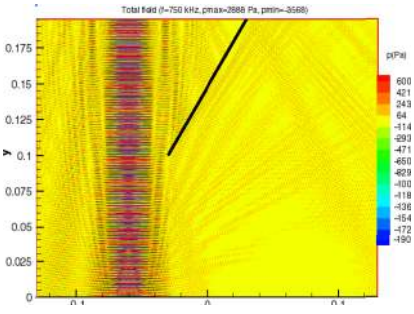

Figure 13. Total Wave Field
(f = 750 kHz)

In summary, high-frequency waves have very different effects on the wafer than the mid-low frequency waves. Because the wave train is limited to a narrow region above the source location, the enhancement of the wafer development process by high frequency agitation depends strongly on the orientation of the wafer and the location of the wafer relative to the acoustic source. In general, vertical immersion of a wafer is less efficient in high frequency agitation than in a mid-low frequency agitation. Since each of the transducer groups at the tank bottom is activated in sequence, there is simply no effect on one side of the wafer when the active transducer strips face the other side. On the contrary, in a mid-low frequency agitation, the acoustic energy will spread to a wider fan-shaped area that reaches at least one side of the wafer. However, for the same power level, lower frequencies are more likely to produce acoustic bubbles that damage fragile features. Thus, to take best advantage of high frequency agitation, the wafer needs to be arranged such that it spends the maximum possible time facing the focused wave region of a sequentially active transducer environment.

DISCUSSION 1. ASYMPTOTIC CYLINDRICAL WAVES IN THE FAR WAVE FIELD

In this section, we will discuss the near and far field character of both mid-low and the high frequency waves. To exclude other factors, only the primary wave field is investigated. The high frequency around 1 megahertz is of primary interest, and the mid-low frequency around 30-40 kilohertz is considered for comparison. The corresponding wavelengths here are around 1.5 mm and 4 cm for high and mid-low frequency, respectively. As already mentioned, 30-40 kilohertz may be considered a high frequency for many other applications.

The reduced potential function of cylindrical waves is a function of phase angle *kr*. As *kr* becomes very large, $kr \gg 1$, an asymptotic expansion of the Hankel function[11] leads to an asymptotic expression for the reduced potential function of the primary field, $\phi_p(x, z)$,

$$kr \gg 1, \qquad H_0^{(2)}(kr) \approx \frac{i(1-i)}{\sqrt{\pi kr}} e^{-ikr} \qquad r = \sqrt{(x - x')^2 + z^2}$$

$$\phi_p(x,z) \approx u_0 \frac{i-1}{2\sqrt{\pi}} \int_{s_1} \frac{e^{-ikr}}{\sqrt{kr}} dx' \qquad u_0 = -\left.\frac{\partial \phi}{\partial n}\right|_{s_1}$$

where S_1 is located at $z = 0$ with a finite width of acoustic source, $n = -z'$. Both of the above equations are valid in the far field region as $r \gg 1 / k = \lambda / (2\pi)$. $1 / k$ is 0.32 mm for the 750 kHz-frequency waves, and is 0.64 cm for the 37.5 kHz-frequency waves. Therefore, the near field regions are all very small and the wafer resides well within in the far field region for both frequencies.

From the above asymptotic expressions, the cylindrical wave is simply a wave of e^{-ikr} in the far field, so the amplitude of ϕ, decays as $(kr)^{-1/2}$. Therefore, the amplitude of the reduced potential is generally smaller for a high frequency wave than for a wave with a lower frequency in the far field due to this factor of $k^{-1/2}$, and the wave-pressure ratio of the two waves is not simply the same as their wave-frequency ratio.

DISCUSSION 2. FOCUSED HIGH FREQUENCY WAVES AND STATIONARY PHASE

Unlike in low frequency waves, high frequency waves form a narrow wave train vertically above the exciting surface. The following derivation helps to explain this behavior in terms of the conventional concept of stationary phase that applies for extremely large value of phase angle kr.

The exponential function in the integral of $\phi_p(x, z)$ changes value rapidly when kr is extremely large. Certainly this is not the case for mid-low frequency waves, but it is true of high frequency waves. In this case, the main contribution to the integral comes from the region where the phase change is zero, that is, the stationary phase domain. To find stationary phase region, it follows from $\partial e^{-ikr}/\partial x' = 0$ that $x' = x$. Thus, it is only around $x' = x$, *i.e.,* right above the excitation source that the exponential function makes a significant contribution to the integral. Regions outside the width of the acoustic source make no significant contribution to the integral because of wave cancellation. As a result, the wave will be focused in a narrow vertical region around $x' = x$, just above the acoustic source.

Now putting $x' = x$ in the integral describing the asymptotic reduced potential function excluding the exponential function, and then representing the exponential function by the first two terms of the Tayor expansion around $x' = x$, it follows that

$$r = z\sqrt{1+\left(\frac{x-x'}{z}\right)^2} \approx z\left[1+\frac{1}{2}\left(\frac{x-x'}{z}\right)^2\right]$$

$$\int_{S_1} \frac{e^{-ikr}}{\sqrt{kr}}dx' \approx \frac{e^{-ikz}}{\sqrt{kz}}\int_{S_1} e^{-\frac{ikz}{2}\left(\frac{x-x'}{z}\right)^2}dx' = -\frac{e^{-ikz}}{\sqrt{kz}}\sqrt{\frac{2z}{k}}\int_{\infty}^{-\infty} e^{-q^2}dq$$

$$= -\frac{e^{-ikz}}{\sqrt{kz}}\sqrt{\frac{2z}{k}}(1-i)\sqrt{\frac{\pi}{2}} = -\frac{\sqrt{\pi}}{k}(1-i)e^{-ikz}$$

The final form of the integral becomes

$$\phi_p(x',z) \approx -\frac{u_o}{2\sqrt{\pi}}(i-1)\frac{\sqrt{\pi}}{k}(1-i)e^{-ikz} = -\frac{u_o}{k}ie^{-ikz}$$

Note that although the limits of the integral are extended outside S_1 to include the entire lower surface from $-\infty$ to ∞, the contributions are negligible in the region where $q^2 \gg 1$.

Therefore, the primary field simply consists of e^{ikz} waves, mostly propagating vertically (in z-direction), and the amplitudes of the waves hardly changes with range. This explains why the high frequency acoustic field and its energy are mainly confined to a narrow region right above the exciting source, and that the amplitude of the waves does not decay, unlike the mid-low frequency cylindrical waves.

Under this approximation, in the far field of a megasonic primary wave, the time average pressure and the time average power intensity thus become

$$\langle p\rangle = \rho\omega\langle\phi\rangle = (1/\sqrt{2})\,\rho\omega\, u_o/k = \rho c\, u_o/\sqrt{2},$$
$$I = \langle pv\rangle = (\langle p\nabla\phi\rangle) = k\langle p\phi\rangle = \rho\omega k\langle\phi\rangle^2 = (1/2)\,\rho\omega\, u_o^2/k = (1/2)\rho c\, u_o^2$$

Surprisingly, these simple expressions indicate that both pressure and power intensity are independent of wave frequency; both depend only on u_o. Pressure ~ u_o and power intensity ~ u_o^2. Figure 14 presents both I curve and rms p curve versus u_0. Therefore, as

shown in Figure 14, a velocity about 0.32 m/s at the surface of transducer strip will result to produce the measured average power density of 7.75 W/cm^2 and an average pressure of 3.35 atm, while 0.2 m/s is probably too small (only corresponding to 2.09 atm and 3 W/cm^2). These analytical approximations can be compared with the numerical calculation of the primary field for 750 kHz. There, a velocity of 0.32 m/s at the transducer surface corresponds to a wave train rms pressure of 3.15 atm and an average power density of 6.8 W/cm^2. These values of pressure and power intensity shown in Figure 14 correspond to a transducer velocity of u_o = 0.30 m/s indicating good agreement with the analytical approximation.

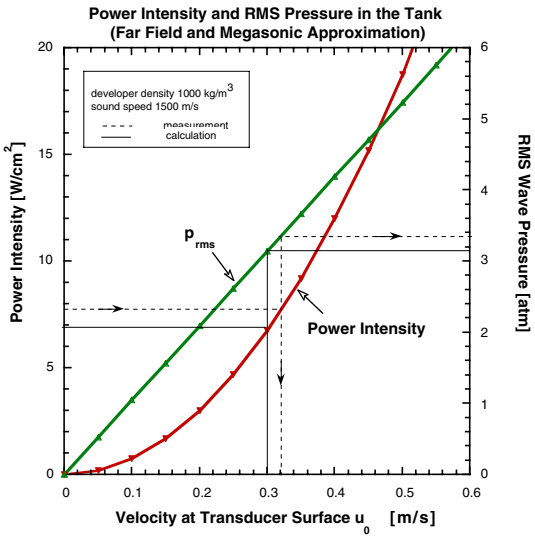

Figure 14. Power Intensity and Pressure in the Tank (Megasonic Far Wave Field Approximation)

MEGASONIC WAVES IN A SINGLE FEATURE CAVITY ON THE WAFER

The wave pressure fields within typical feature cavities are solved separately from the tank problem, because of their very small length scale. In a sequential active transducer set up, the waves generated in a feature cavity by each transducer in a full time cycle (in which all transducer strips are sequentially activated once) may be integrated in time to obtain the average agitation in a time cycle. In this work we begin by addressing the field produced by one activated transducer strip.

The wafer surface is initially flat during development, all of the feature cavities of the designed microstructure gradually take shape as the exposed regions are dissolved by the liquid developer. As in the tank problem, the half space Green's function is used to

construct the primary wave field, and the free space Green's function is used to construct the reflected wave field. The total wave field in a single feature cavity is then computed as the summation of the primary and the reflected wave fields.

In the early stage when the cavity is very shallow, the agitation is very effective since there are almost no obstacles to block primary wave beams. However, as the depth of the cavity increases, primary waves may no longer reach the entire cavity surface. Depending on the orientation of the wafer relative to the acoustic source, part of the cavity will be in the shadow region of the primary wave field unless the primary wave beams are about parallel to the sidewalls of the cavity. The shadow region can only be filled by the reflected waves, including not only the first reflections but also the subsequent reflected waves. Because the width of the cavity is generally much smaller than the acoustic wavelength, the series of reflected waves hardly decay between reflections. In this work, only the first reflected waves are included with the understanding that subsequent reflections may contribute substantially to the total field.

Wave reflection within the cavity is considered at every wall of the cavity and at the wafer surface, but the tank walls are too distant to be included. The dependence of boundary for a field point inside the cavity is much simpler than in the tank problem, for it will always include the cavity bottom and sidewalls.

Example: Pressure Waves in a Slender Cavity for a favorable case

Figures 15 gives the layout of a wafer in a tank, and the location of a feature cavity on the wafer face. Figure 16 shows the root mean square (rms) wave pressure in the feature cavity for the primary, reflected, and the total wave fields, respectively, for 750 kHz agitation. The single feature is selected as a 50 μm $\times$ 400 μm cavity (aspect ratio 8) with its mouth located at the wafer center. The wafer is at a 29.8-degree angle to the tank bottom, almost perpendicular to the line extended from the wafer center to the acoustic source. At this angle the cavity bottom can "see" almost the entire acoustic source, so the primary waves from the acoustic source (at 0.052 m to 0.076 m on tank bottom) will fill most of the cavity.

The shadow region in the primary field is very narrow and can be identified on the left of line L_2, where L_2 is the wave beam emitted from the very right end of the acoustic source. L_1 is the wave beam emitted from the very left end of the acoustic source, and it reaches the cavity right wall at about its 2/3 length. In the fan shaped region between these two lines (L_1 and L_2), there is a complicated interference-wave-pattern produced by the crossing of primary waves near the left corner of the cavity mouth. Note that the blue region to the right of line L_2 of the primary field has essentially the same rms pressure as the wafer face outside the cavity. This pressure is relatively low because the cavity is located neither right above the acoustic source (layout in Figure 15) nor at the local wave peaks (Figure 17).

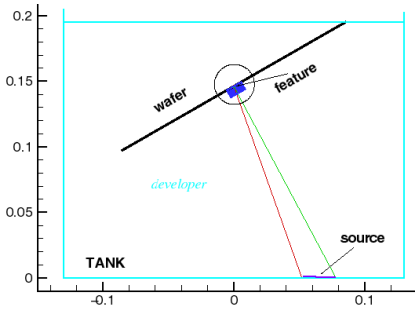

Figure 15. Sketch of Layout

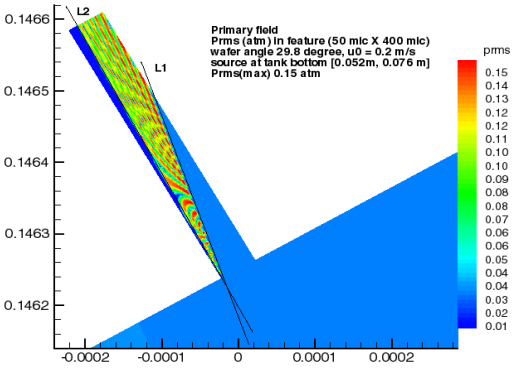

a) Primary Field

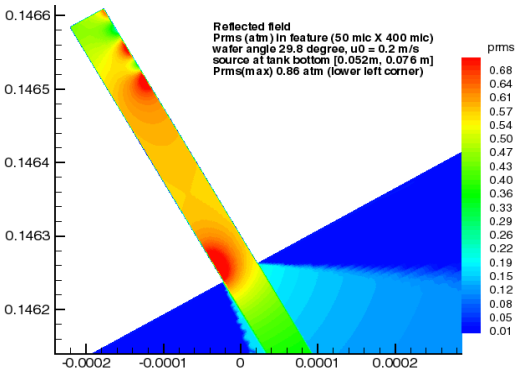

b) Reflected Field

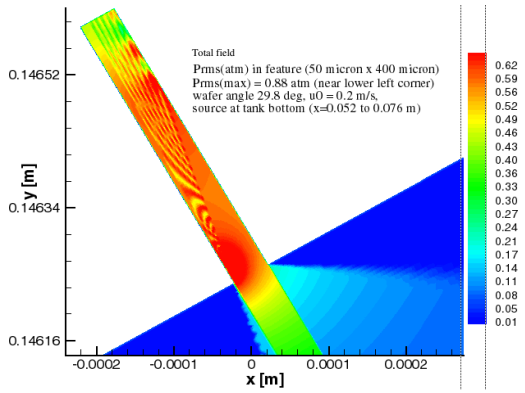

c) Total Field

Figure 16. RMS Wave Pressure in a Single Cavity

The reflected waves in the cavity are emitted from the cavity right-wall, most of the cavity bottom wall, and the left corner of the cavity mouth. Because the cavity width and depth are all smaller than the wavelength, there is no wave cancellation and the superposition of reflected waves results in a great enhancement of the wave pressure — a wave trapping phenomena. Thus, the magnitude of the resulting total pressure field is

much larger than that of the primary field. Reflected waves emitted from the cavity also greatly enhance the wave pressure in the region immediately outside the mouth. The strongest rms pressure occurs near the left corner of the cavity mouth, where all of the reflected waves emitted from cavity walls and from acoustic source overlap in a very small spot. For similar reasons, wave pressures are also large at some spots on the right cavity wall.

Figure 17 shows the primary, reflected, and the total pressure wave fields in the liquid adjacent to the wafer face. Note that the area covered in Figure 17 is the small rectangular area in the circled region just beneath the wafer (the blue area in Figure 15). The angle between primary waves and those reflected waves from the wafer is small due to the 33in the primary field.

Despite the relatively low primary pressure of 0.13 atm at the feature mouth in Figure 16 and 17, reflections within the cavity can produce remarkably large rms pressures. For a 0.2 m/s disturbance velocity at the transducer surface, the maximum rms pressure in Figure 16 is as high as 0.88 atm at left corner of cavity mouth, much stronger than the pressure immediately outside the cavity mouth, and double the maximum pressure in the tank, 0.42 atm. This is because that at that corner point, convergent primary waves overlap with reflected waves from all cavity walls. Since these large pressures imply large fluid velocities, acoustic agitation may provide considerable benefit even for features well outside the primary focused wave train.

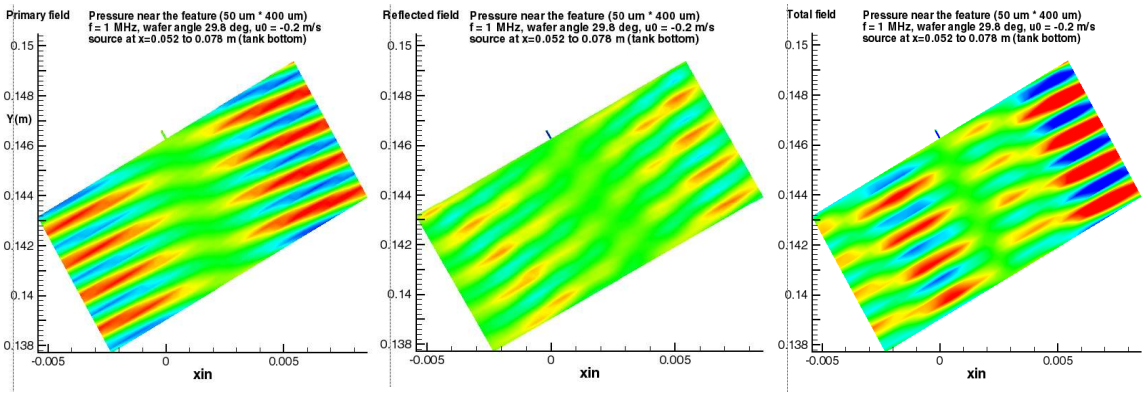

Figure 17. Primary, Reflected, and Total Wave Fields Near the Feature Cavity
Wafer Angle 29.8 degree

Example: Pressure Waves in a Slender Cavity for an Unfavorable Case

When the wafer is inclined at another angle, 41.5 degree, relative to the tank bottom, the cavity bottom cannot "see" the acoustic source. In this case, primary waves can only reach a small part of the right cavity wall, and the maximum total rms wave pressure is only around 0.16 atm for a 750 kHz agitation, more than four times smaller than that of the previous case. This results from a large shadow region in primary field and a short boundary length reached by the primary waves. The reflected waves emitted from the short boundary length cannot fill a large shadow region, so most of the field remains relatively weak at least for a single reflection. Figure 18 gives the total wave pressure field of this case. Note that the contour plots in this figure describe the instantaneous pressure amplitude instead of rms wave pressure.

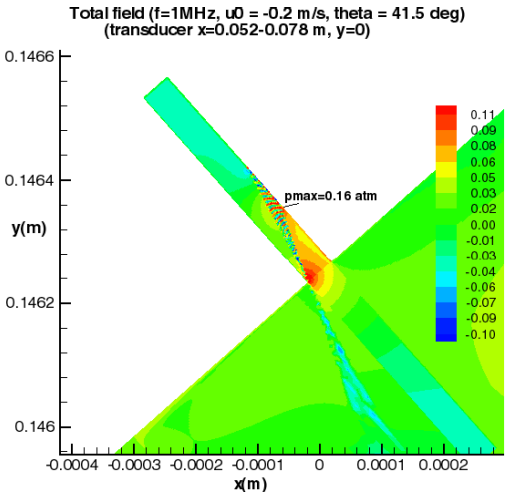

Figure 18. Total Wave Pressure Field in a Slender Cavity (wafer angle 41.5 degree)

Figure 19 shows the primary, reflected, and total wave fields in the region around the feature. Because of the wafer orientation, the total field has more peaks at each wave front than seen earlier in Figure 17. The reason for this is that the angle between the primary and reflected waves is larger than in the previous case, so the resulting interactions create more peaks in the direction perpendicular to the wave travel.

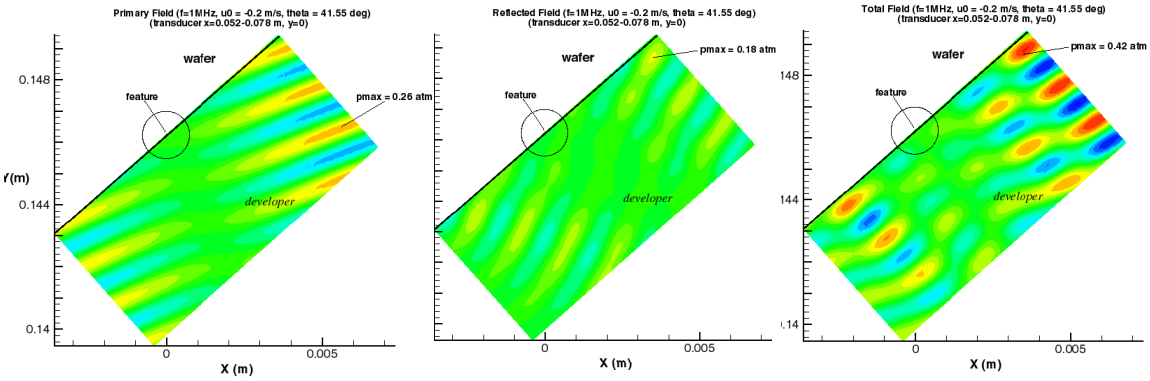

Figure 19. Primary, Reflected, and Total Wave Fields Near a Feature Cavity
Wafer angle 41.5 degree

Example: Pressure Waves in a Short Cavity

To see how the aspect ratio of a cavity will influence the internal wave pressure, a shorter cavity (same width and half-depth) with the same wafer orientation (41.5 degree) and acoustic source is investigated. Figure 20 gives the total pressure field in the short cavity. It is seen that the wave pattern in the cavity is almost the same as that in the slender cavity except that the fractional area of the shadow region is much smaller than before. Therefore, even though the cavity bottom cannot "see" the acoustic source, the reflected waves are stronger than that in the slender cavity. The maximum wave pressure on the right wall is 0.42 atm for the total field. This is almost the same as the maximum wave pressure in the tank and more than double the maximum pressure of the slender cavity.

In the three preceding examples, the feature cavities are not located within or near the primary wave train but instead lie well outside the wave train, and the feature mouth is not coincident with the acoustic wave peak. Thus, the reported results probably underestimate the acoustic pressure in more favorably oriented features.

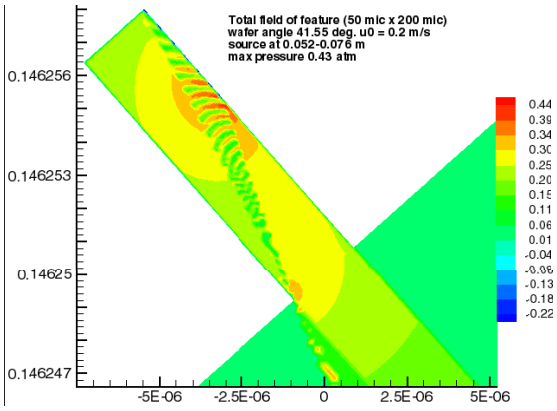

Figure 20. Total Wave Pressure Field in a Short Cavity (Wafer angle 41.5 degree)

SUMMARY AND DISCUSSION

Analytical and numerical methods have been employed to investigate acoustic wave fields used to enhance the development of LIGA photoresists. Pressure waves within the development tank and within individual feature cavities are solved separately using spectral methods based on Green's functions and Green's identity. The primary and reflected wave field are constructed in sequence and then added to obtain the total wave field, rather than solving large systems of algebraic equations. The most difficult task is to treat the interference of the wafer with the wave fields in the tank. This difficulty is overcome by identification of shadow region in the primary field based on optical ray tracing and by using a similar strategy to discern the boundary of dependence of the reflected field.

Second and higher order reflected waves are not included in the present simulations. This is permissible in a tank with dimensions much greater than the acoustic wavelength because the divergence of cylindrical and spherical waves greatly reduces the amplitude of successive reflections. First reflections are generally weaker than primary waves. Second reflections are weaker yet, and so on. In the feature-scale problem, however, the first reflected wave field and the subsequent reflected fields can be almost as strong as the primary wave field, since the cavity is much smaller than a megasonic wavelength. Here, the second reflected wave field and beyond may make important contributions to the total wave pressure. These currently neglected higher-order reflections can only add to the wave energy of the current lower bound estimates.

The results of the calculations provide valuable physical insights which were previously unknown to us. In contrast to the divergence of low frequency waves, megasonic waves are characterized by a narrowly focused wave train just above the acoustic source. This numerical expectation was verified analytically and recently confirmed by experimental data obtained by the Sandia LIGA Group.[13] As a result, the LIGA development process will be greatly accelerated, if the orientation and location of the immersed wafer are arranged so that the wafer spends more time in a focused high frequency wave field. Thus, a vertically submerged wafer may not be the best choice when the driving

transducers are mounted in the tank floor. Perhaps, this is the reason why German workers have arranged sidewall acoustic sources in a tank for a vertically submerged wafer. On the other hand, a lower agitation frequency may alternatively be used to produce a broader but weaker wave field. However, care must be taken in reducing the frequency since this allows more time for the growth of acoustic bubbles that may damage fragile features. Another possible approach is the alteration of transducer duty cycles or the use of baffles to better focus the wave energy of all transducers onto the wafer face. More work needs to be done to determine the wafer orientations that will produce optimal results. The tools developed here will be used to investigate these alternative pathways toward improvement of LIGA development.

In this work we have assumed that the wafer is rigid, permitting wave reflections but no transmission. However, the importance of wave transmission has been recently demonstrated by Forschungzentrum Karlsruhe, using back-side impingement of acoustic waves to enhance development, we intend to next investigate the acoustic response of an elastic wafer.

REFERENCES

1. R. H. Nilson, S. K. Griffiths, Acoustic Agitation for Enhanced Development of LIGA PMMA Resists, *Proceedings of the SPIE Symposium on Micromachining and Microfabrication Process Technology*, V1, 14174, No. 5, 2000.

2. T. Iwamoto, H. Shimada, S. Shimomura, M. Onodera, and T. Ohmi, High Reliability Lithography Performed by Ultrasonic and Surfactant- Added Developing System, *Jpn. J. Appl. Phys,* Vol. 33, Pt. 1. No. 1B, 1994.

3. K. L. Lee, J. Bucchignano, J. Gelome, and R. Viswanathan, Ultrasonic and Dip Resist Development Processes For 50 nm Device Fabrication, *J. Vac. Sci. Technol.* **B** 15 (6), Nov/Dec 1997.

4. J. M. Ryan, A. C. F. Hoole, and A. N. Broers, A Study of the Effect of Ultrasonic Agitation During Development of Poly(Methyl-Methacrylate) for Ultrahigh Resolution Electron-Beam Lithography, *J. Vac. Sci. Technol*. **B** 13 (6), Nov/Dec 1995.

5. J. Zanghellini, S. Achenbach, A. El-Kholi, J. Mohr, and F. J. Pantenburg, New Development Strategies for High Aspect Ratio Microstructures', *Microsystem Technologies* **4**, 94–97, 1998.

6. PCT Systems, Inc, Instruction Manual for Tiger Tank Hyperclean Megasonic Cleaning System, October 1996.

7. LMS International, SYSNOISE , a commercial acoustic software, Belgium, 1987.

8. S. Dahnke and F. J. Keil, Modeling of Three-Dimensional Linear Pressure Fields in Sonochemical Reactors with Homogeneous and Ihomogeneous Density Distributions of Cavitation Bubbles, *Ind. Eng. Chem. Res*., Vol 57, No. 5, 1998.

9. G. S. Kino, *Acoustic Waves: Devices, Imaging, and Analog Signal Processing*, Preentice-Hall, Inc., 1987.

10. G. F. Roach, *Green's Functions: Introductory Theory With Applications*, New UniversityMathematics Series, 1970. L. C. Andrews, *Special Functions of Mathematics For Engineers*, Oxford University Press, 1998.

11. L.C. Andrews, *Special Functions of Mathematics For Engineers*, Oxford University Press, 1998.

12. F. J. Fahy, *Sound Intensity*, Elsevier Applied Science, 1989.

13. D. Larsen, M. Bankert, Experimental Study of Acoustic Agitation for Enhanced LIGA Resist Development, Sandia LIGA Group, Sandia Technical Seminar, September, 2001.

DISTRIBUTION:

1	MS 0329	E. J. Garcia, 2614
1	MS 0329	A. D. Oliver, 2614
1	MS 0503	D. W. Plummer, 2330
1	MS 0603	T. R. Christenson, 1743
1	MS 0826	W. L. Hermina, 9113
1	MS 0834	K. S. Chen, 9114
1	MS 0834	J. E. Johannes, 9114
1	MS 0835	S. N. Kempka, 9141
1	MS 0835	J. M. McGlaun, 9140
1	MS 9001	M. E. John, 8000 Attn: D. R. Henson, 8400 MS 9007 J. Vitko, 8100, MS 9004 W. J. McLean, 8300, MS 9054 P. N. Smith, 8500, MS 9002 K. E. Washington, 8900, MS 9003
1	MS 9042	G. H. Evans, 8728
1	MS 9042	S. K. Griffiths, 8728
1	MS 9042	M. F. Horstemeyer, 8728
1	MS 9042	W. G. Houf, 8728
1	MS 9042	R. S. Larson, 8728
1	MS 9042	C. D. Moen, 8728
1	MS 9042	R. H. Nilson, 8728
10	MS 9042	A. Ting, 8728
1	MS 9401	M. A. Bankert, 8729
1	MS 9401	J. M. Hruby, 8702
1	MS 9401	J. T. Hachman, 8729
1	MS 9401	C. Henderson, 8729

1	MS 9401	R. P. Janek, 8729
1	MS.9401	A. M. Morales, 8729
1	MS 9401	R. Shediac, 8729
1	MS 9401	D. M. Skala, 8729
1	MS 9405	R. H. Stulen, 8700 Attn: R. Q. Hwang, 8721, MS 9161 W. R. Even, 8722, MS 9403 J. C. F. Wang, 8723, MS 9403 C. H. Cadden, 8724, MS 9402 J. R. Garcia, 8725, MS 9404 E. P. Chen, 8726, MS 9161 P. A. Spence, 8727, MS 9042
1	MS 9405:	K. L. Wilson, 8703
1	MS 9409	H. A. Bender, 8730
1	MS 9671	D. A. Chinn, 8729
3	MS 9017	Central Technical Files, 8945-1
1	MS 0899	Technical Library, 9616
1	MS 9021	Classification Office, 8511/Technical Libarary, MS 0899, 9616
1	MS 9021	Classification Office, 8511 for DOE/OSTI via URL


Sandia National Laboratories